Exp Fluids (2016) 57:150
DOI 10.1007/s00348-016-2233-6

RESEARCH ARTICLE

An experimental study on the aeromechanics and wake characteristics of a novel twin-rotor wind turbine in a turbulent boundary layer flow

Zhenyu Wang[1] · Wei Tian[1] · Ahmet Ozbay[1] · Anupam Sharma[1] · Hui Hu[1]

Received: 10 August 2015 / Revised: 22 July 2016 / Accepted: 17 August 2016 / Published online: 2 September 2016

Abstract The aeromechanic performance and wake characteristics of a novel twin-rotor wind turbine (TRWT) design, which has an extra set of smaller, auxiliary rotor blades appended in front of the main rotor, was evaluated experimentally, in comparison with those of a conventional single-rotor wind turbine (SRWT) design. The comparative study was performed in a large-scale wind tunnel with scaled TRWT and SRWT models mounted in the same incoming turbulent boundary layer flow. In addition to quantifying power outputs and the dynamic wind loadings acting on the model turbines, the wake characteristics behind the model turbines were also measured by using a particle image velocimetry system and a Cobra anemometry probe. The measurement results reveal that, while the TRWT design is capable of harnessing more wind energy from the same incoming airflow by reducing the roots losses incurred in the region near the roots of the main rotor blades, it also cause much greater dynamic wind loadings acting on the TRWT model and higher velocity deficits in the near wake behind the TRWT model, in comparison with those of the SRWT case. Due to the existence of the auxiliary rotor, more complex vortex structures were found to be generated in the wake behind the TRWT model, which greatly enhanced the turbulent mixing in the turbine wake, and caused a much faster recovery of the velocity deficits in the turbine far wake. As a result, the TRWT design was also found to enable the same downstream turbine to generate more power when sited in the wake behind the TRWT model than that in the SRWT wake, i.e., by mitigating wake losses in typical wind farm settings.

✉ Hui Hu
huhui@iastate.edu

[1] Department of Aerospace Engineering, Iowa State University, Ames, IA 50010, USA

1 Introduction

Most of utility-scale wind turbines in nowadays are in single-rotor wind turbine (SRWT) design, which has three rotor blades mounted onto a hub at front of a turbine nacelle. While the long rotor blades of the turbines are aerodynamically optimized in outboard region, the blade sections near turbine hub (i.e., roots of blades) are designed primarily to withstand structural loads (i.e., bending and torsional). Therefore, very high thickness-to-chord ratio airfoils, which are aerodynamically poor, are usually used at turbine roots to provide structural integrity. Such a configuration results in a "dead" zone near rotor axis where virtually no wind energy is extracted from the incoming airflow. Up to 5 % loss in wind energy extraction capability is estimated to occur per turbine due to such structure compromise at the roots of turbine blades (Selvaraj et al. 2013; Rosenberg et al. 2014). These "root losses" occur even for wind turbines that operate in isolation, i.e., with no other turbine nearby.

Wind turbines sited in modern wind farms are usually arranged in an organized pattern. Due to the wake interferences of upwind turbines, the downstream turbines located in the wake regions of the upstream turbines would see very different incoming surface wind profiles, in comparison with the upwind turbines. As described in Vermeer et al. (2003), a turbine wake can usually be divided into two regions, i.e., a near wake and a far wake. While turbine near wake is the region from the turbine rotor disk to the downstream location within the first diameter of the turbine rotor, the far wake refers to the region at further downstream

beyond the near wake. While the flow characteristics in the turbine near wake are mainly determined by the aerodynamics and the number of rotor blades (i.e., attached or separated flows around the rotor blades, generation and shedding of unsteady tip and root vortices), the actual shape of turbine rotor blades is not important in the far wake and the research topics for far wake flows are primarily focused on turbulence models, wake interference and topographical effects. Extensive studies have been conducted to examine the wake characteristics behind wind turbines in recent years. For examples, while Whale and Anderson (1993), Massouh and Dobrev (2007), Grant and Parkin (2000), and Sherry et al. (2013) studied the flow characteristics in the near turbine wakes with model turbines placed in uniform incoming airflows or water flows, Chamorro et al. (2011), Hu et al. (2011), Yang et al. (2011), Tian et al. (2014), Howard et al. (2015) and Xie and Archer (2015) investigated the evolution of the unsteady wake vortex structures behind wind turbines sited in turbulent boundary layer flows. Chamorro and Porté-Agel (2008, 2009), and Sescu et al. (2015) investigated the effects of thermal stability and boundary layer turbulence on the turbine wake characteristics. Ross and Ainslie (1981) and Yuan et al. (2014) found that the velocity deficits in a turbine wake over a flat surface would recover rapidly within the first six rotor diameters (i.e., up to 70 %), and then recovered gradually at further downstream region (e.g., reach nearly 80 % at the downstream of 8D). Barthelmie et al. (2003) and Hansen et al. (2012) conducted field measurements in an offshore wind farm and reported that the velocity deficits in the turbine wake would recover only 10 to 45 % when the spacing between the wind turbines being 1.7D to 7.4D in the offshore wind farm. They also found that the recovery of the velocity deficits in the turbine wake would be very slow when the spacing between the turbines being exceeds 6.5D. More recently, Tian et al. (2014) performed a wind tunnel study to examine the effects of turbulence levels of the incoming airflows on the recovery rate of the wake velocity deficits behind wind turbines. They found that the wake velocity deficits would recover much faster with a higher turbulence level in the incoming boundary layer flow (i.e., for the cases in typical onshore wind farms with turbulence intensity level being ~20 % at the turbine hub height), in comparison with that with relatively low turbulence level in the incoming airflow (i.e., for the cases in typical offshore wind farms with turbulence intensity level being ~10 % at the turbine hub height). Cal et al. (2010) and Lebron et al. (2010) investigated the interactions between wind turbine arrays and boundary layer flows to reveal the vertical transport of momentum and kinetic energy across the boundary layer into the wind turbine arrays.

Lu and Porté-Agel (2011), Ozbay et al. (2012), and Chamorro and Porté-Agel (2011) investigated the turbulence properties of turbine wake flows inside and above aligned and staggered wind farms and found that the recovery rate of the velocity deficits and the turbulence characteristics of turbine wake flows would affect the dynamic wind loadings and power production of the downstream wind turbines greatly. Since a portion of the kinetic energy of the incoming airflow has already been harnessed by the upstream turbines, the downstream turbines would see much lower incoming wind speed, thereby, less wind energy available for the downstream turbines, in comparison with the upstream turbines. The power losses of the downstream turbines due to the wake interference from upstream turbines are usually called *wake losses,* which have been found to be about 20–40 % in typical wind farms (Barthelmie et al. 2007, 2009; Storm et al. 2009; Barthelmie et al. 2010; Yuan et al. 2014). The primary mechanism of the wake losses is due to the ingestion of low-momentum wake from upstream turbines by the downstream turbines. The wake losses were found to be strong dependent of farm location, layout pattern, and stability conditions of the atmospheric boundary layer (ABL) winds. The highest wake losses have been observed in offshore wind farms when wind turbines are closely spaced, and aligned well with the incoming airflow direction (Wan and Wu 2004; Barthelmie et al. 2007; Barthelmie et al. 2010; Hansen et al. 2012; Wu and Porté-Agel 2015).

While the significance of the "root" and "wake" losses is evident by the magnitudes as described above, even a small improvement in reducing the losses for given wind farm configurations and atmospheric climates is economically significant. According to Barthelmie and Jensen (2010), 1 % increase in power output of a 100 MW wind farm would be equivalent to approximately $0.5 million/year increase in revenue. In comparison with the large body of the previous studies which were mainly devoted to measuring and predicting "root losses" or/and "wake losses", very little can be found in the literature to explore effective strategies for root loss reduction or/and wake loss mitigation. Corten et al. (2007) suggested a method of farm control in which upstream turbines are deliberately yawed with respect to wind direction. The concept aims to use the lateral force (generated by deliberate yawing of upstream turbines) to divert the flow away from downstream turbines. More recently, Yuan et al. (2014) evaluated the effects of relative rotation directions of turbine rotors on the power production performances of the wind turbines when arranged in tandem. They found that the turbines in counter-rotating configuration would harvest more wind energy from the same incoming wind, in comparison with the case in co-rotating configuration.

In the present study, we report our recent efforts to explore a novel twin-rotor wind turbine (TRWT) concept to improve power production of individual turbines as well as wind farm efficiency. The TRWT concept employs an additional set of

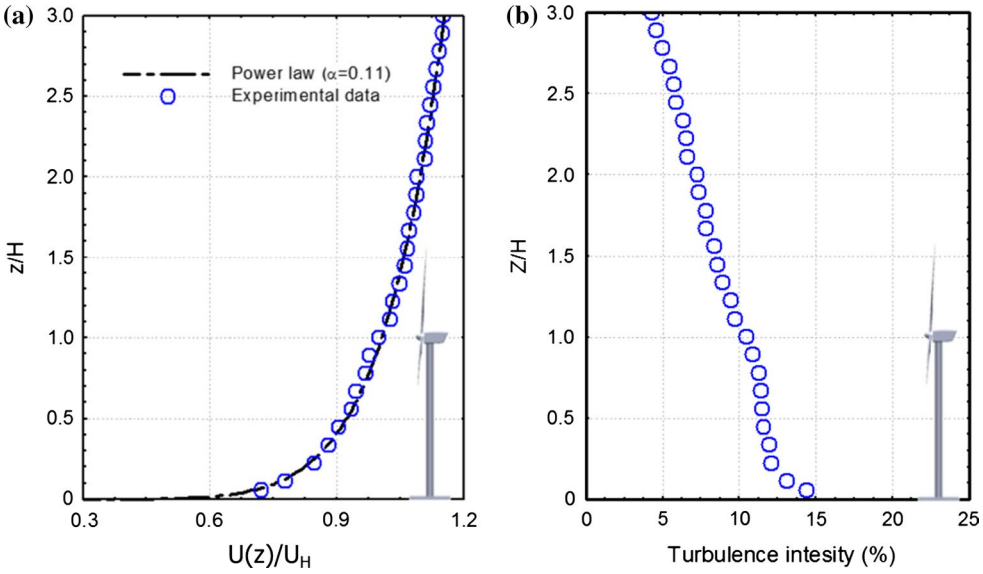

Fig. 1 Flow characteristics of the incoming boundary layer airflow used for the present study. **a** Mean streamwise velocity profiles; **b** Turbulence intensity profiles

smaller, co-axial auxiliary rotor blades with two objectives: (1) to improve power production of individual turbines by reducing the root losses incurred in the root region of the main rotor blades; and (2) to mitigate wake losses in wind farm settings through rapid mixing of turbine wake. Mixing rate of TRWT wakes will be enhanced by (a) increasing radial shear in turbine wake flows and (b) using dynamic interaction among the unsteady wake vortices shedding from the primary and auxiliary rotors. The experimental study was performed in a large-scale atmospheric boundary layer (ABL) wind tunnel located at Iowa State University (ISU). Scaled TRWT and SRWT models were placed in a same turbulent ABL wind under neutral stability conditions. In addition to measuring dynamic wind loads acting on the model turbines, a digital particle image velocimetry (PIV) system was used to quantify the evolution of the unsteady wake vortices (i.e., formation, shedding and breakdown) and turbulent mixing process in the turbine wake flows. The power outputs of a same model turbine sited in the wake behind the TRWT model at different downstream locations were also measured and compared quantitatively with those sited in the turbine wake behind the SRWT model. The detailed flow measurements were correlated with the dynamic wind loading and power output data in order to gain further insight into underlying physics for improved power production and durability of wind turbines.

2 Experimental setup and test models

2.1 Atmospheric boundary layer (ABL) wind tunnel used in the present study

The experimental study was conducted in a large-scale Aerodynamics/Atmospheric Boundary Layer (AABL) wind tunnel available at the Aerospace Engineering Department of Iowa State University (ISU). The AABL tunnel, which has a test section of 20 m in length, 2.4 m in width and 2.3 m height with optically transparent side walls, is capable of generating a maximum wind speed of 45 m/s in the test section. During the experiments, a model wind turbine was mounted in the center of the test section. Chain arrays were placed on the floor of the wind tunnel test section at the upstream of the wind turbine model to trigger the turbulent boundary layer of the incoming airflow to simulate the ABL winds over typical wind farms. Further information about the generation and characterization of the ABL flow in the AABL tunnel is available at Tian et al. (2014).

As described in Kaimal and Finnigan (1994), Jain (2010), and Zhou and Kareem (2002), the velocity profile of a typical ABL wind over a wind farm can be expressed by using a power function, i.e., $U(z) = U_H (Z/H)^{\alpha}$, where U_H is the wind speed at a reference height of H (i.e., turbine hub height for the present study). The power-law exponent "α" is a function of the terrain roughness. Figure 1 gives the measured velocity and turbulence intensity profiles of the incoming boundary layer airflow in the test section of the AABL tunnel used for the present study. The measured mean velocity data were found to be fitted well with a power function with the power-law exponent $\alpha \approx 0.11$, which agrees well with the ISO standard for offshore ABL wind profile (i.e., $\alpha \approx 1/8.4$). The measured turbulence intensity of the incoming airflow at the turbine hub height was found to be about 10 %, which also agrees with the field measurement data reported in Hansen et al. (2012) for the wind turbines in Horns Rev offshore wind farm. For comparison, Tong (2010) suggested that the typical turbulence intensity levels for offshore wind turbines would be about 8 %. To follow up the work of Røkenes (2009), the

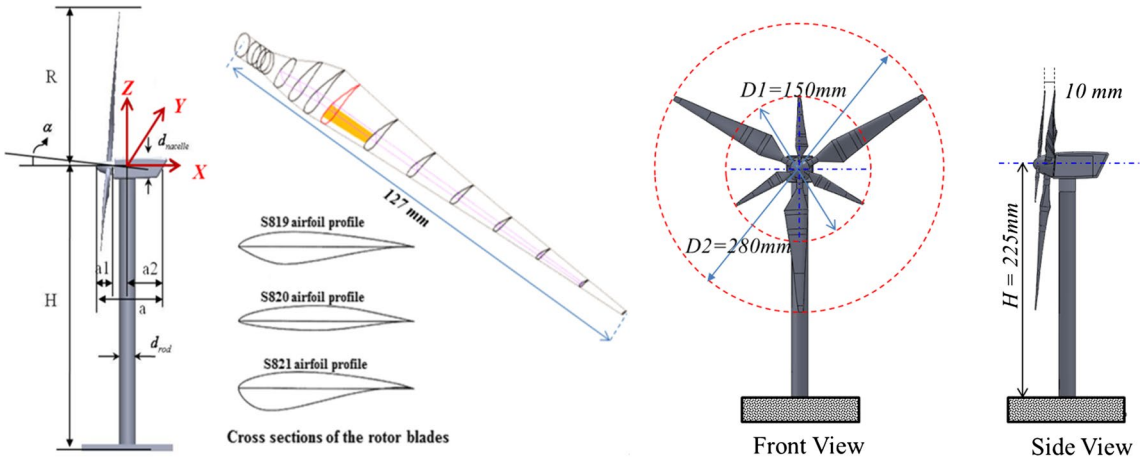

(a) Schematic of the SRWT model. **(b)** Schematic of the SRWT model.

Fig. 2 Schematic of the SRWT and TRWT models used in the present study

Table 1 The design parameters of the wind turbine models used in the present study

Parameter	R	H	D_{rod}	$D_{nacelle}$	α	a	a_1	a_2
Dimension (mm)	140	225	18	26	5°	68	20	35

integral length scale of the incoming turbulent airflow at the turbine hub height (i.e., H = 225 mm above the wind tunnel floor) was estimated to be about 200 mm for the present study, which agrees well with the values reported in Røkenes (2009).

2.2 Wind turbine models

Figure 2 shows a schematic of the wind turbine models used for the present study. The SRWT model has a hub height of $H = 225$ mm and a rotor diameter of $D = 280$ mm. With a scale ratio of 1:320, the turbine model is used to represent a utility-scale turbine with a hub height of 80 meters and rotor diameter about 90 meters (i.e., ~2 MW turbines usually seen in modern wind farms). All the parts of the test model are made of a hard plastic material by using a rapid prototyping machine. The rotor blades of the turbine model are designed with ERS-100 turbine blades (Locke et al. 2004) as the prototype. A direct current (DC) generator (Kysan, FF-050S-07330) was installed inside the turbine nacelle, which can produce electricity when driven by the rotating turbine blades. While the primary design parameters are listed in Table 1, further information about the SRWT model is available in Tian et al. (2014).

As shown in Fig. 2b, the TRWT model is made by adding a set of smaller, auxiliary blades in front of the main rotor blades. The auxiliary rotor blades have the same airfoil geometry as the main rotor blades, but with a down-scaled ratio of 2:1. While two sets of the rotor blades were mounted onto the same hub (i.e., to drive the same shaft of the DC generator sited inside the turbine nacelle), the auxiliary rotor blades and main rotor blades were arranged in a staggered pattern along azimuthal direction with the auxiliary rotor blades being at 10 mm upstream of the main rotor blades.

In the present study, the incoming airflow velocity at the turbine hub height was maintained at $U_H = 6.5$ m/s. The corresponding chord Reynolds number of the model turbines (i.e., based on the wind speed at the turbine hub height and averaged chord length of the main rotor blades) was found to be about 9000 (i.e., $Re_C \approx 9000$), which is much lower than those of the utility-scale turbines (i.e., $Re_C > 1.0 \times 10^6$). As described in Alfredsson et al. (1982), while the working Reynolds number of a turbine may affect its power production performance, the flow characteristics in turbine wakes were found to become almost independent of Reynolds numbers when the Reynolds numbers becoming high enough. More recently, Chamorro et al. (2012) proposed to utilize the Reynolds number, Re_D, which is defined by using the wind speed at the turbine hub (U_H) and turbine rotor diameter (D), to characterize turbine wake flow statistics. They found that mean velocity in a turbine wake would reach Reynolds number independence at $Re_D \approx 4.8 \times 10^4$ and that of higher-order flow statistics started at $Re_D \approx 9.3 \times 10^4$. For the test cases of the present study, the Reynolds number, Re_D, is about 120,000, which is greater than the required minimum value to reach Reynolds number independence for turbine wake statistics as suggested in Chamorro et al. (2012).

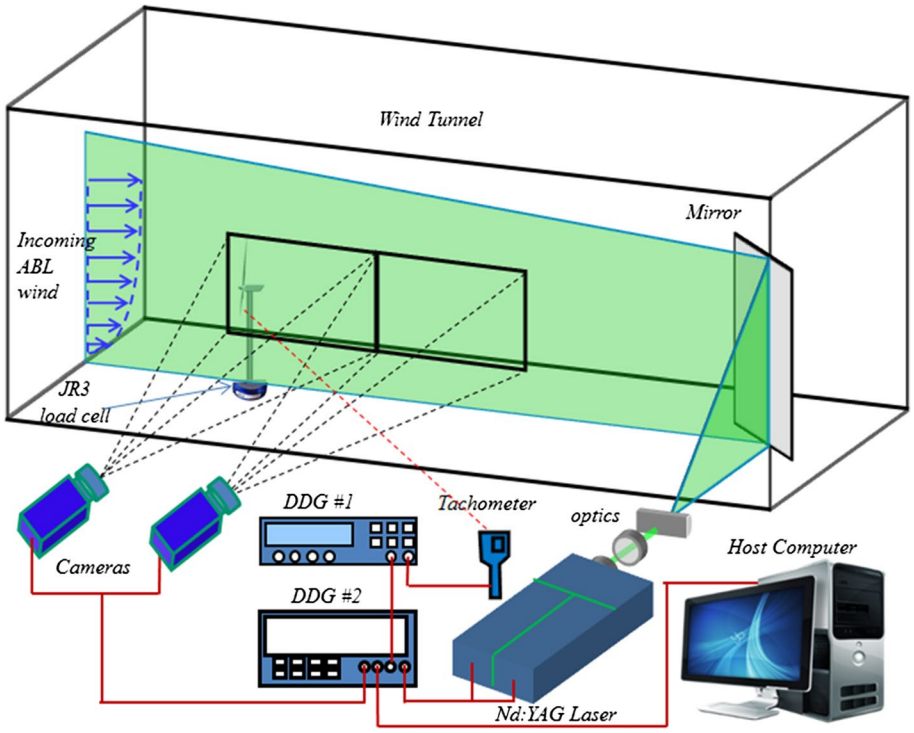

Fig. 3 Experimental setup used for PIV measurements

2.3 Dynamic wind loading and power output measurements

For the turbine models used in the present study, circular aluminum rods were used to support the turbine rotors, hubs and nacelles. Through holes on the floor of the wind tunnel test section, the circular aluminum rods were connected to high-sensitivity load cells (JR3 load cells, model 30E12A-I40) to measure the dynamic wind loadings acting on the test models. The JR3 load cell is capable of measuring instantaneous aerodynamic forces and the moments about each axis with a measurement uncertainty levels being smaller than ±0.25 % of the force measurement range (40 N). In the present study, the dynamic wind loadings acting on the turbine models were measured at a sampling rate of 1000 Hz with the duration of 60 s for each test case. The resonant frequencies of the load cells were monitored during the experiments, which were found to be much higher than the rotation frequencies of the wind turbines.

During the experiments, a Monarch tachometer was also used to measure the rotation speed of the wind turbine blades. By applying different electric loads to the electric circuits connected to the DC generators installed inside the turbine nacelles, the rotation speeds of the turbine rotors were adjusted in the range of 0 to 2200 rpm, and the corresponding tip-speed ratio (*TSR*) of the model turbines was found to be $TSR = 0$–6.5. The power outputs of the model turbines were determined by measuring the voltage outputs of the DC generators inside the turbine nacelles and corresponding electric currents in the electric circuits. For the test models used in the present study, the optimum tip-speed ratio of the model turbine was found to be about 5.0 (i.e., the model turbines were found to have the maximum power outputs at $TSR \approx 5.0$). For comparison, a typical utility-scale wind turbine operating in modern wind farms usually has a tip-speed-ratio value of $TSR \approx 4.0$–8.0, as described in Burton et al. (2001).

2.4 PIV measurements to quantify the wake characteristics behind the model turbines

A digital particle image velocimetry (PIV) system was used in the present study to conduct detailed flow field measurements to quantify the flow characteristics of the wake flows behind the turbine models. Figure 3 illustrates the experimental setup for the PIV measurements. A fog generator was used to generate small oil droplets of ~1 μm in size to seed the incoming boundary layer airflow. A double-pulsed Nd:YAG laser (EverGreen200, BigSky Corp.) with a pulse energy of 200 mJ/pulse at the wavelength of 532 nm was used as the illumination source. A set of mirrors along with spherical and cylindrical lenses were used to shape the laser beam into a laser sheet of ~1.0 mm in thickness to illuminate the tracer particles seeded in the airflow. Two high-resolution digital cameras (PCO1600, Cooke Corp) were used for PIV image acquisition in order to have a larger measurement window to reveal the evolution of the unsteady wake vortex structures behind the model turbines.

The digital cameras and the double-pulsed Nd:YAG lasers were connected to a host computer via a digital delay generator (Berkeley Nucleonics, Model 565), which controlled the timing of the pulsed laser illumination and image acquisition for PIV measurements. During the experiments, the PIV image acquisition rate was selected to a frame rate that is not a harmonic frequency of the rotation speed of the turbine rotor blades in order to determine the ensemble-averaged flow quantities (e.g., mean flow velocity, TKE, and Reynolds shear stress) of the turbine wake flows.

For PIV image processing, a cross-correlation algorithm with interrogation window size of 32 × 32 pixels and an effective overlap rate of 50 % was used to derive instantaneous flow velocity vectors from the acquired PIV images. The ensemble-averaged flow characteristics in the terms of mean flow velocity, in-plane turbulence kinetic energy (i.e., $TKE = 0.5 * (\overline{u'^2} + \overline{v'^2})/U_H^2$), and normalized Reynolds shear stress (i.e., $\overline{\tau} = -\overline{u'v'}/U_H^2$) were determined based on about 1000 frames of instantaneous PIV measurements for each test cases. For the PIV measurement results given in the present study, the measurement uncertainty level was estimated to be within 2 % for the flow velocity vectors, while that of the ensemble-averaged flow quantities such as turbulent kinetic energy and Reynolds shear stress is about 5 %.

During the experiments, "Phase-locked" PIV measurements were also performed to reveal further details about the evolution of the unsteady wake vortices behind the model turbines in relation to the positions of the rotating rotor blades. For the "Phase-locked" PIV measurements, a digital tachometer, which can generate a pulsed signal as a pre-marked turbine rotor blade at a pre-selected position, was used to trigger the digital PIV system via a Digital Delay Generator (DDG). By putting different time delays between the input signal from the tachometer and the output signal from the DDG, the "phase-locked" PIV measurements with the pre-marked rotor blade at different rotation positions (i.e., at different rotation phase angles) were accomplished. 400 frames of instantaneous PIV measurements at the same phase angle were used to calculate the phase-averaged flow velocity and vorticity distributions in the turbine wake flows.

In addition to the PIV measurements, a Cobra anemometry system (Turbulent Flow Instrumentation Pty LtD) was also used to achieve time-resolved flow velocity measurements at the points of interest (i.e., in the turbine wake of X/D = 2, 4, 6, and 8) to supplement the near wake PIV measurements. The Cobra anemometry system has a 4-hole pressure probe that can measure all 3-components of flow velocity and local static pressure in excess of 2.5 kHz within a ±45° cone of acceptance. Further technical information about the cobra anemometry system is available at http://www.turbulentflow.com.au/Products/Products.php. In the present study, the Cobra anemometry system was used to conduct flow velocity measurements at each prescribed points with a data sampling rate of 2.5 kHz for 60 s.

3 Measurement results and discussions

3.1 Dynamic wind loadings acting on the wind turbine models

In the present study, the dynamic wind loading measurements were conducted with the TRWT and SRWT models mounted in the same incoming boundary layer airflow and operating at their optimum tip-speed ratios (i.e., where the power outputs of model turbines reaching their peak values). Figure 4 shows typical wind loading measurement results in the term of instantaneous thrust coefficients. While only the measured thrust coefficient was presented here, similar features were also revealed by the other components of the measured aerodynamic forces and moments. In the present study, the thrust coefficient, C_T, and corresponding bending moment coefficient, C_M, were defined as $C_T = F_x/\left(0.5\rho U_H^2 \pi R^2\right)$ and $C_M = M_z/\left(0.5\rho U_H^2 \pi R^2 H\right)$, respectively, where ρ is the density of air, R is the radius of the main rotor of turbine models, and T is the thrust force acting on the turbine models. The mean values (i.e., the time-averaged values) of the thrust coefficients were also given in the plots as the dashed lines for comparison. As shown clearly in Fig. 4, the dynamic wind loadings acting on the model turbines were found to fluctuate significantly as a function of time. While the TRWT and SRWT models were mounted in the same incoming boundary layer flow, the dynamic wind loads acting on the TRWT model were found to become greater (i.e., both the mean values and the fluctuation amplitudes) than those acting on the SRWT model, due to the existence of the additional auxiliary rotor blades.

Based on the time sequences of the instantaneous wind loading measurements as those shown in Fig. 4, the mean and standard deviation values of the dynamic wind loadings acting on the two model turbines were determined, which are listed in Table 2. It can be seen clearly that due to the existence of the auxiliary rotor for the TRWT model, while the mean wind loadings acting on the TRWT model increased slightly (i.e., ~16 % increase in both the time-averaged thrust force and mean bending moment), the standard deviation values of the dynamic wind loadings acting on the TRWT model were found to increase much more significantly (i.e., ~75 % increase in the dynamic thrust force, and 140 % more in the dynamic bending moment), in comparison with those acting on the SRWT model.

It should also be noted that as described in Tian et al. (2014), the standard deviation of the dynamic wind

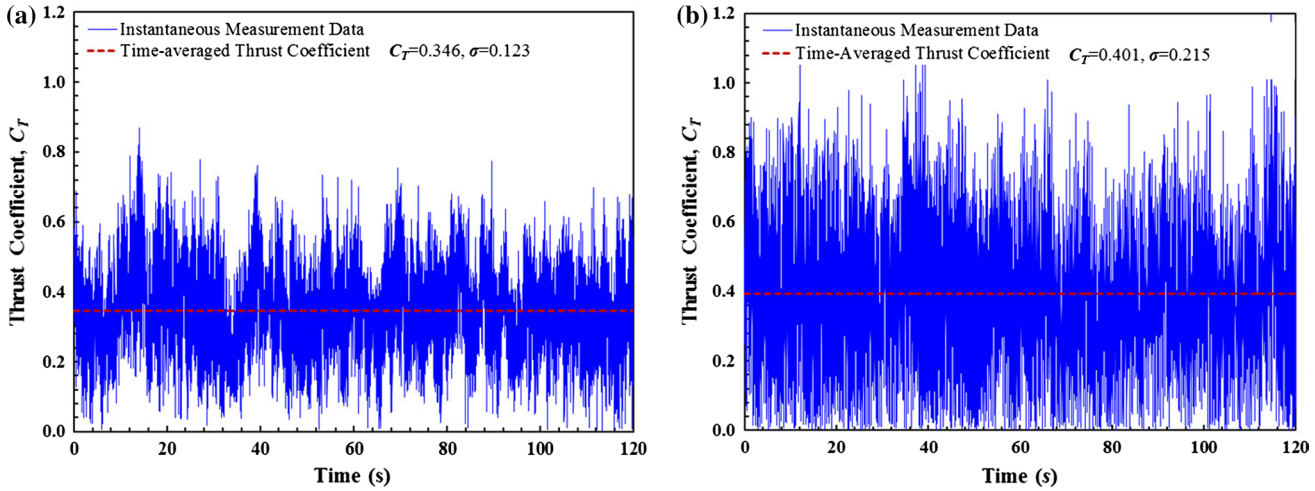

Fig. 4 Time history of the instantaneous thrust forces acting on the SRWT and TRWT models. **a** Thrust coefficients of the SRWT model; **b** Thrust coefficients of the TRWT model

Table 2 The dynamic wind loadings acting on the SRWT and TRWT models

Wind load measurement results	SRWT	TRWT
Mean thrust coefficient, C_T	0.346	0.401
The standard deviation of the thrust coefficient, σ_{CT}	0.123	0.215
Mean bending moment coefficient, C_M	0.411	0.475
The standard deviation of the bending moment coefficient, σ_{CM}	0.133	0.324

loadings can be used as a quantitative parameter to evaluate the fatigue loadings acting on the wind turbines. In comparison with those of the SRWT case, the much larger fluctuations of the dynamic wind loadings would indicate much severe fatigue loadings acting on the TRWT models. This is believed to be closely related to the more complex wake vortex structures and higher TKE levels in the wake behind the TRWT model, which were revealed clearly from the PIV measurement results to be discussed in the next session.

3.2 PIV measurements to reveal the wake flow characteristics behind the TRWT model

Figure 5 shows the PIV measurement results in the term of the ensemble-averaged flow velocity distributions in the near wakes behind the SRWT and TRWT models. It can be seen clearly that since a portion of the kinetic energy of the incoming flow was harvested by the wind turbines, the magnitudes of the flow velocity in the turbine wakes were found to become much smaller than those of the incoming flow. The existence of a region with relatively high velocity in the near wake behind the SRWT is revealed clearly

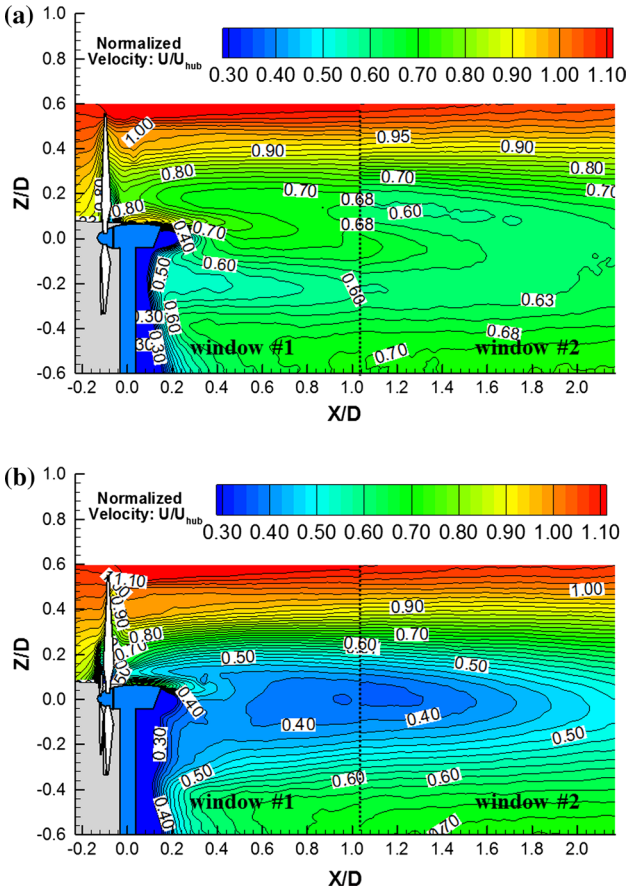

Fig. 5 Ensemble-averaged velocity distributions the SRWT and TRWT models. **a** The wake behind the SRWT model; **b** The wake behind the TRWT model

from the PIV measurement result at the region right above the turbine nacelle (i.e., near the roots of the turbine rotors at the region of Z/D < 0.2, and extending up to X/D = 0.5

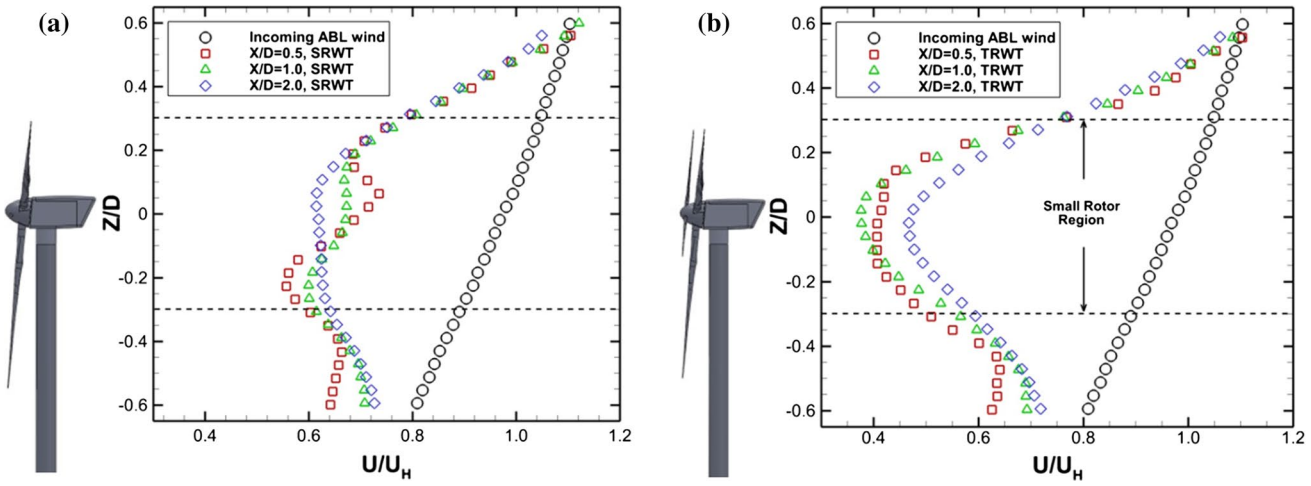

Fig. 6 Vertical velocity profiles in the wakes behind the SRWT and TRWT models. **a** In the wake of the SRWT model; **b** In the wake of the TRWT model

downstream). This is believed to be due to the aerodynamically poor design at the root regions of the rotor blades for the SRWT (i.e., the blade roots are designed mainly to provide structural integrity, instead of harvesting wind energy). For the TRWT case, since the smaller auxiliary rotor blades were appended in front of the main rotor blades to reduce the root losses, the flow velocity behind the TRWT model were found to become much smaller, especially in the region near the roots of the main rotor blades.

Figure 6 illustrates the vertical profiles of streamwise velocity extracted from the ensemble-averaged PIV measurement results at the downstream locations of $X/D = 0.5$, 1.0 and 2.0, respectively. The mean velocity profile of the incoming flow was also plotted in the plots for comparison. It can be seen clearly that comparing with the velocity profile of the incoming flow, significant velocity deficits were found in the turbine near wakes due to the existence of the turbine rotor blades. In comparison with those behind the SRWT model, the velocity deficits behind the TRWT model were found to be much more significant, especially in the downstream of the sweeping area of the smaller auxiliary rotors near the roots of the main rotor blades. Based on the conservations of momentum and energy as described in Hu et al. (2011), with the TRWT and SRWT models mounted in the same incoming airflow, the larger velocity deficits in the near wake behind the TRWT model would indicate a greater thrust force acting on the TRWT model as well as a better power production performance of the TRWT design, in comparison with those of the SRWT case. While the stronger wind loads acting on the TRWT model were revealed quantitatively from the measurement results given in Table 2, the improved power production performance of the TRWT design is due to the existence of the smaller auxiliary rotors to reduce the root losses of the main rotor blades.

Based on the measurement results given in Fig. 6a, it can also be seen that very little changes can be observed among the vertical profiles of streamwise velocity extracted at different downstream locations behind the SRWT model up to $X/D = 2.0$. It indicates that the velocity deficits in the wake behind the SRWT model would need a much longer distance to recover. However, as shown in Fig. 6b, while the velocity deficits behind the TRWT model were also found to recover very slowly in the near wake region (i.e., $X/D \leq 1.0$ region), the recovery of the velocity deficits was found to become much faster in the far wake region (i.e., $X/D > 1.0$ region). The much faster recovery of the velocity deficits in the far wake behind the TRWT model is believed to be closely related to the generation of more complex wake vortex structures and enhanced turbulent mixing due to the existence of the auxiliary rotor, which were revealed clearly from the measured TKE and turbulent Reynolds stress distributions in the TRWT wake flow given in Figs. 7 and 8.

Figure 7 shows the normalized in-plane turbulent kinetic energy (TKE) distributions in the turbine wake flows, which can provide further insights to explain the differences in the recovery of the wake velocity deficits behind the two compared turbine models. Lignarolo et al. (2014) and Tian et al. (2014) suggested that the evolution of the unsteady wake vortices (i.e., generation, shedding, breakdown and dissipation) would play an important role on the TKE production in a turbine wake. As shown clearly in Fig. 7, the regions with relatively high TKE levels were found to concentrate in the wake flows immediately behind the turbine towers and nacelles due to the formation and shedding of unsteady wake vortices from the turbine nacelles and towers. The TKE levels were also found to be quite high at the upper regions behind the rotation disks of the turbine rotor

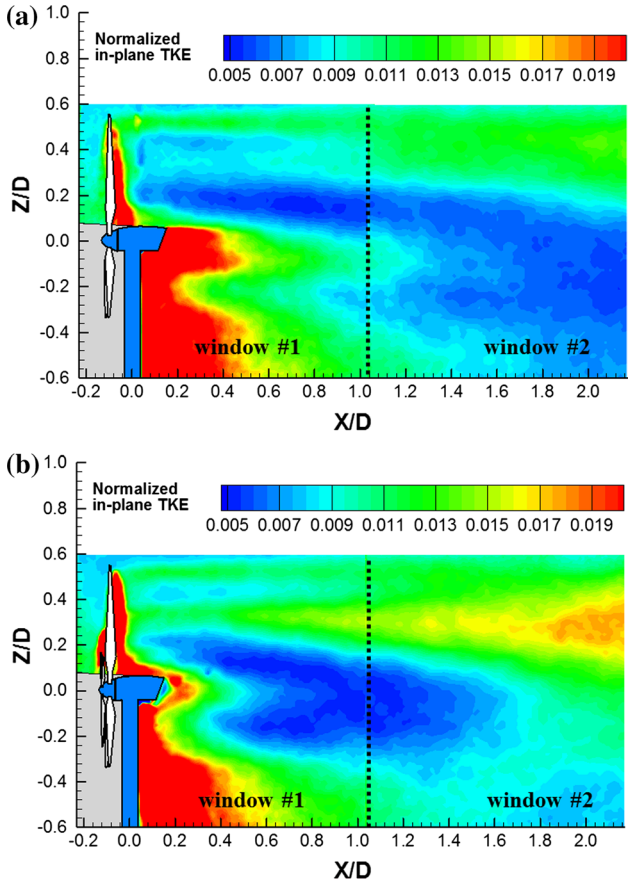

Fig. 7 Normalized TKE distributions in the wake flows behind the SRWT and TRWT models. **a** Normalized TKE distribution behind the SRWT model; **b** Normalized TKE distribution behind the TRWT model

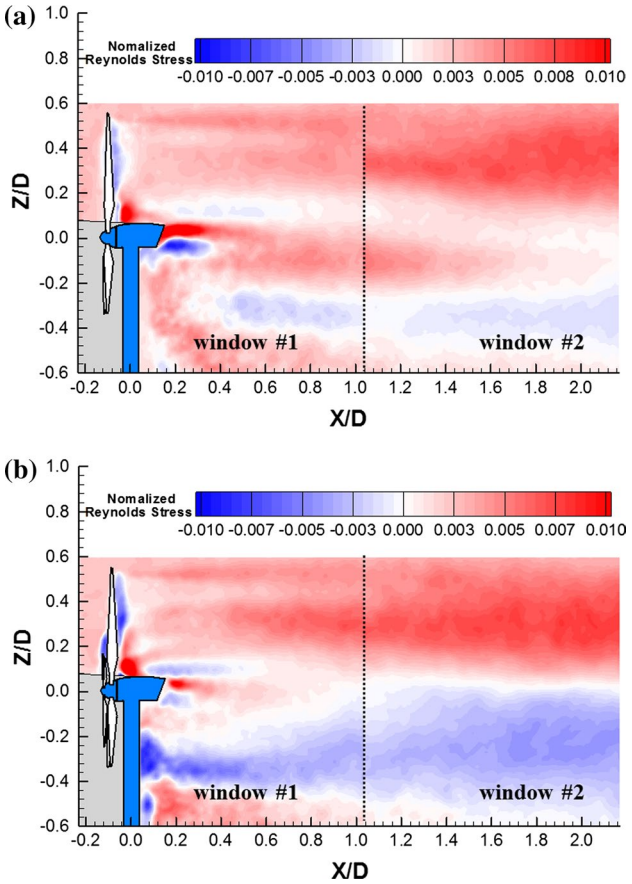

Fig. 8 Reynolds shear stress distributions behind the SRWT and TRWT models. **a** Behind the SRWT model; **b** Behind the TRWT model

blades, which is correlated well to the shedding paths of the tip vortices at the tips of the rotating blades. The expansion of the turbine wakes with the increasing downstream distance was also seen clearly from the TKE distributions.

While the TKE distribution pattern in the wake flows behind the two turbine models was found to be quite similar in general, some obvious differences can also be identified from the comparison of the TKE distributions behind the TRWT and SRWT models. Corresponding to the tip vortex shedding from the smaller auxiliary rotor blades, an additional region with relatively high TKE levels was also found to exist in the wake behind the TRWT model (i.e., X/D < 1.0), in comparison with those behind the SRWT model. The onsets of the tip vortex breakdown (i.e., the starting points of the regions with much higher *TKE* levels as described in Tian et al. (2014)) were also found to be quite different in the wakes behind the TRWT and SRWT models. While the breakdown of the tip vortices in the wake behind the TRWT model was found to take place earlier than the SRWT case, the absolute TKE values in the wake behind the TRWT model were become greater than those in the SRWT wake, especially in the region of X/D > 1.0. As suggested by Tian et al. (2014), since the TKE level can usually be used as an indicator to evaluate the extent of turbulent mixing in a turbulent flow, the higher TKE levels in the TRWT wake would indicate more intensive mixing in the wake flow, resulting in the faster recovery of the velocity deficits in the wake behind the TRWT model. It should also be noted that the absolute TKE values along the shedding paths of the tip vortices in the near wake region (i.e., $X/D < 1.0$) were found to be relatively low in general, where concentrated tip vortices were observed in the "phase-locked" PIV measurement results to be discussed later. The measurement results were found to agree well with the findings reported in Medici (2005), who suggested that the concentrated tip vortices would act as a shield preventing turbulent mixing and TKE production in the near wake behind a wind turbine.

Meneveau and his co-workers (Lebron et al. 2010; Calaf et al. 2010; Cal et al. 2010; Meyers and Meneveau 2012) conducted a series of experimental and numerical studies

on the wake characteristics behind wind turbines and suggested that the energy extracted from a turbine array is less a matter of wind passing through one turbine to the next, but more of turbulence created behind one turbine drawing down high velocity wind from above. Wu and Porte-Agel (2012), Calaf et al. (2010) and Cal et al. (2010) also suggested that the Reynolds stress levels in a turbine wake would play a very important role in promoting the vertical transport of the kinetic energy from above into a turbine wake. Higher Reynolds stress levels in a turbine wake will draw down more high velocity airflow from above to "re-charge" the low-momentum wake flow behind the wind turbine.

Figure 8 shows the measured Reynolds stress distributions in the wakes behind the SRWT and TRWT models. As shown clearly in the figures, the regions with relatively higher levels of Reynolds shear stress were found to exist in the turbine wakes at the top tips of the turbine main rotors, similar to the *TKE* distributions given in Fig. 7. As the downstream distance increases, the Reynolds shear stress levels in the turbine wakes were found to increase rapidly. Higher levels of the Reynolds shear stress were also observed in the wakes behind the turbine towers and nacelles, corresponding to the generation and shedding of unsteady vortex structures in these regions. While the general features of the Reynolds stress distributions in the wakes behind the two compared turbine models were found to be quite similar, the absolute values of the Reynolds shear stress in the wake behind the TRWT model were found to be greater than those of the SRWT case, especially in the far wake region (i.e., X/D > 1.0).

Based on the comparisons of the *TKE* and Reynolds stress distributions described above, it can be seen clearly that due to the existence of the smaller auxiliary rotor appended in front of the main rotor blades, the *TKE* and Reynolds shear stress levels in the wake behind the TRWT models were found to become much higher than those of the SRWT case, especially in the far wake region (i.e., X/D > 1.0). As suggested by Wu and Porte-Agel (2012), Calaf et al. (2010)and Cal et al. (2010), the higher *TKE* and Reynolds shear stress levels in the turbine wake would indicate more intensive mixing in the wake flow, which would cause a faster vertical transport of kinetic energy by entraining more high-speed airflow from above to re-charge the lower momentum wake flow behind the TRWT model. As a result, the velocity deficits in the wake behind the TRWT model would recover much faster than those behind the SRWT model, especially in the region of X/D > 1. The faster recovery of the velocity deficits in the far wake behind the TRWT model was revealed more clearly from the measurement results of the Cobra anemometer system in the turbine far wakes, which will be discussed later.

3.3 "Phase-locked" PIV measurements to reveal the evolution of the turbine wake vortices

As described above, "phase-locked" PIV measurements were also conducted in order to reveal the evolution of the unsteady vortices in the turbine wakes in relation to the phase angle of the turbine rotor blades more clearly. The phase angle of $\theta = 0.0°$ refers the situation with the pre-marked rotor blade in the most upward position. As the phase angle increases, the pre-marked rotor blade would rotate out of the vertical PIV measurement plane. Figures 9 and 10 give the "phase-locked" PIV measurement results in the term of the vorticity distributions in the turbine wakes at the phase angles of $\theta = 0.0°$, 30.0°, 60.0°, and 90.0°, respectively. It can be seen clearly that the wake flows behind the turbine models are actually very complex vortex flows, which filled with various unsteady vortices in different sizes and orientations.

As shown clearly in Fig. 9, a tip vortex would be induced in the wake flow behind the SRWT model from the tip of the pre-marked rotor blade at the phase angle of $\theta = 0.0°$. As the phase angle increases, the tip vortex was found to shed from the tip of the pre-marked rotor blade. As indicated by the oblique dashed lines in the figures, the tip vortices were found to align themselves nicely along with other tip vortices induced by other rotor blades to form moving tip vortex arrays in the turbine wake. An additional row of concentrated vortex structures were also found to be generated in the wake flow at approximately 60–70 % span of the turbine rotor blades. The vortex structures were found to move outward with the expansion of the SRWT wake flow, merging with the tip vortex structures and dissipated eventually further downstream. Similar wake vortex structures at approximately 60–70 % span of the rotor blades were also observed in the previous studies of Hu et al. (2011), Tian et al. (2014) and Whale et al. (2000). It can also be seen that unsteady vortices would also be generated and shed periodically from the roots of the turbine rotor blades as root vortices. Other wake vortex structures, such as those generated over the upper and lower surfaces of the turbine nacelles as well as the unsteady von-Karman vortex streets shedding from the turbine towers, can also be seen clearly from the phase-locked PIV measurement results. As described in Tian et al. (2014), the flow characteristics in the turbine wake were found to be dominated by the evolution (i.e., formation, shedding, breakdown and dissipation) of the unsteady wake vortices.

Due to the existence of the auxiliary rotor blades appended in front of the main rotor blades, the wake vortex structures behind the TRWT model were found to become more complicated, in comparison with those behind the SRWT model. As shown in Fig. 10, in addition to the wake vortex structures similar as those behind the SRWT model (i.e., the tip and root vortices shedding from tips and roots

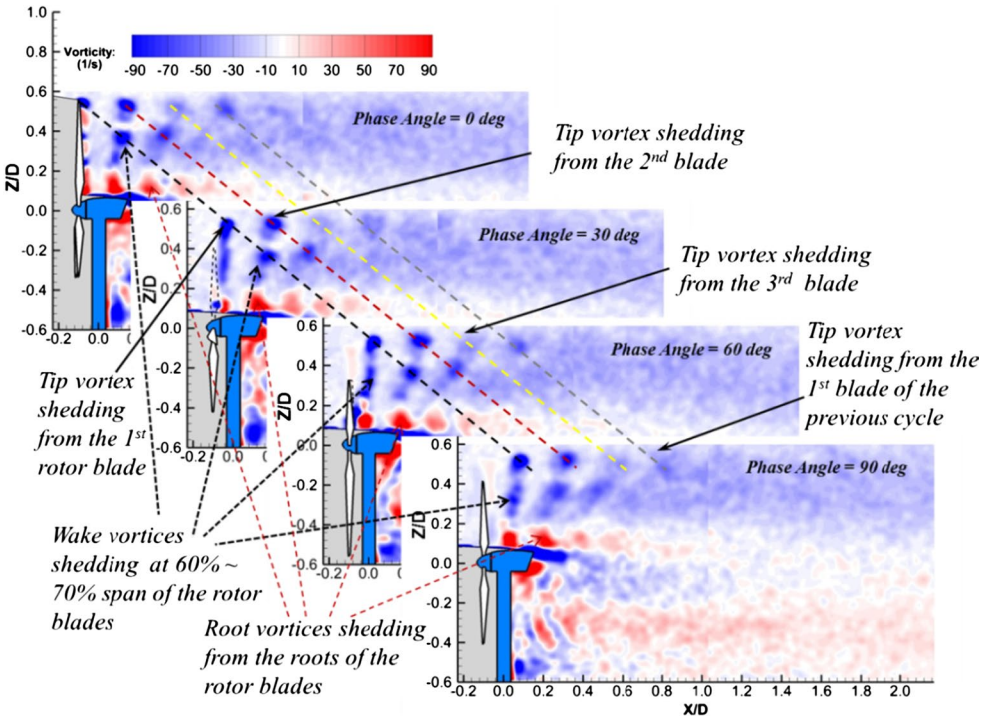

Fig. 9 Phase-locked PIV measurement results in the wakes behind the SRWT model

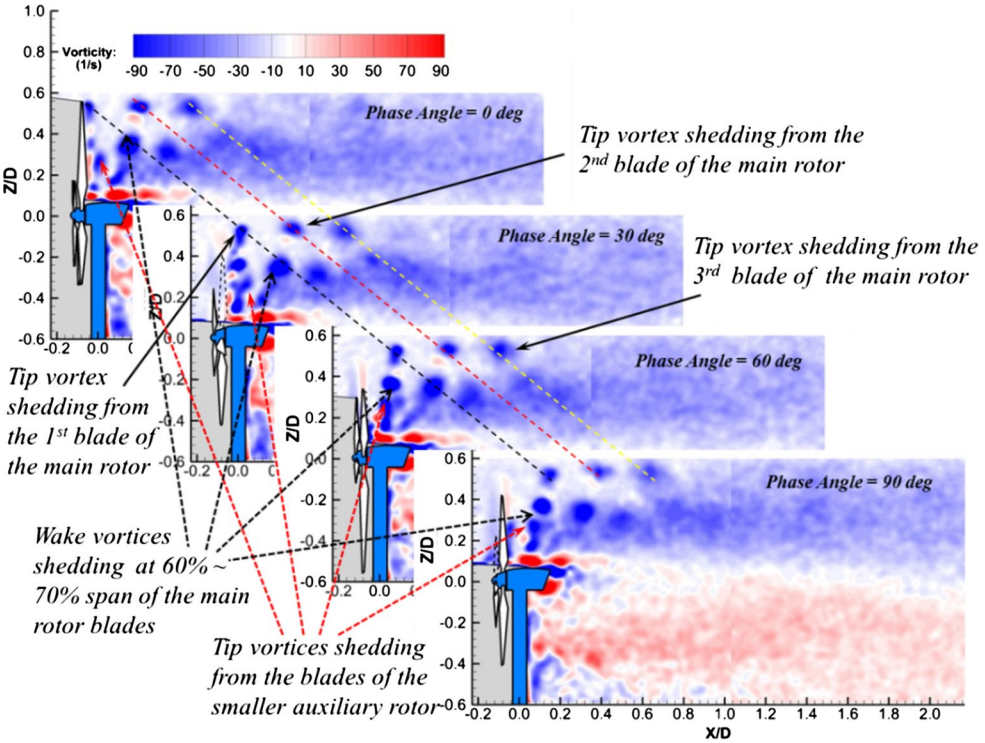

Fig. 10 Phase-locked PIV measurement results in the wakes behind the TRWT model

of the main rotor blades, the concentrated wake vortices at 60–70 % blade span of the main rotor, and unsteady vortices shedding from the turbine nacelle and tower), a new set of wake vortices were also found to be generated and shed periodically from the tips of the smaller auxiliary rotor blades of the TRWT model. Induced by the new tip vortices shedding from the tips of auxiliary rotor blades, the concentrated vortices at 60–70 % span of the main rotor blades were found to move inward as they travel downstream in the wake behind the TRWT model, whereas the vortex structures were found to move outward for the SRWT case. The root vortices shedding from the roots of the main rotor blades were also

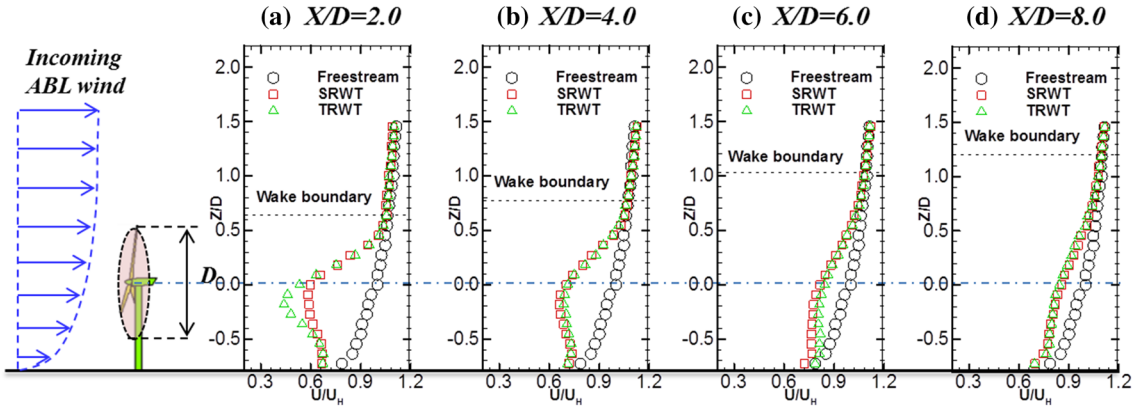

Fig. 11 Streamwise velocity profiles in the wakes behind the SRWT and TRWT models

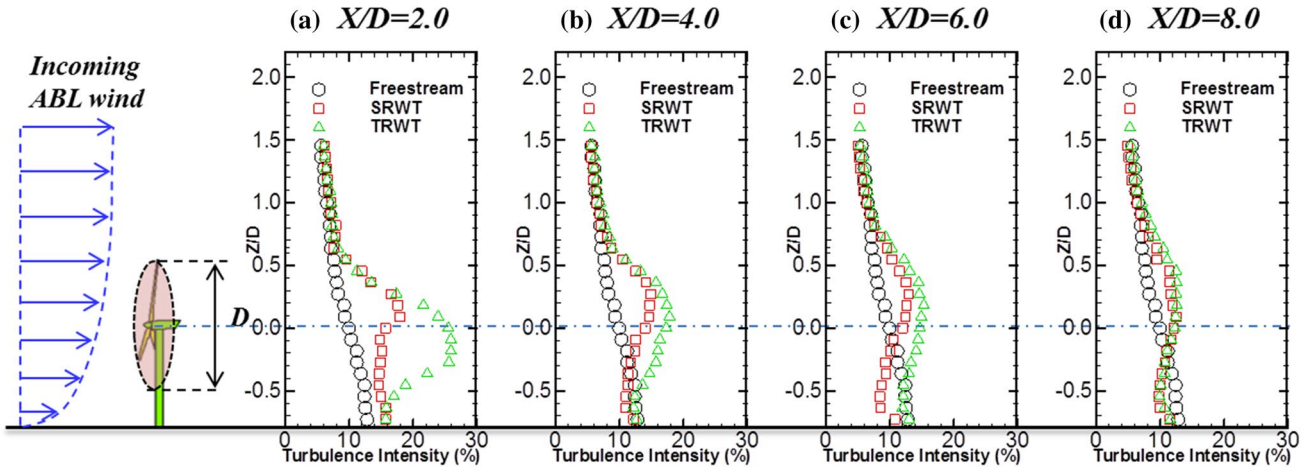

Fig. 12 Turbulence intensity profiles in the wakes behind the SRWT and TRWT models

found to become smaller and weaker due to the existence of the auxiliary rotor blades. Corresponding to the more complicated interactions among the wake vortices behind the TRWT model, the breakdown of the concentrated tip vortices and the wake vortices at 60–70 % span of the main rotor blades were found to take place earlier in the wake behind the TRWT model (i.e., vortex breakdown at $X/D \approx 0.6$ for the TRWT case, while at $X/D \approx 0.9$ for the SRWT case). The earlier breakdown of the concentrated wake vortices in the wake behind the TRWT model was found to be in good agreement with the earlier appearance of the regions with elevated TKE and Reynolds stress levels in the wake behind the TRWT model, as shown in Figs. 7 and 8.

3.4 Flow characteristics in the far wakes behind the TRWT model

As described above, a Cobra anemometry system was also used in the present study to conduct flow velocity measurements in the turbine far wakes to supplement the near wake PIV measurements. Figures 11 and 12 give the measured vertical profiles of the streamwise velocity and turbulence intensity in the far wakes behind the SRWT and TRWT models (i.e., at the downstream locations of X/D = 2.0, 4.0, 6.0 and 8.0, respectively). The streamwise velocity and turbulence intensity profiles of the incoming airflow were also given in the plots for comparison.

As described above, with the smaller auxiliary rotor appended in front of the main rotor, the TRWT design would be able to harness more wind energy from the same incoming airflow by reducing the root losses of the main rotor blades. As a result, the incoming flow was found to decelerate more severely in the near wake behind the TRWT model, especially in the region near the roots of the main rotor blades, in comparison with that of the SRWT case. The greater velocity deficits in the wake flow near the TRWT model were also revealed quantitatively from the measurement results of the Cobra anemometry system

at the downstream of location of $X/D = 2.0$, as given in Fig. 11a. The measured turbulence intensity profiles given in Fig. 12a reveal clearly that the turbulence intensity levels in the wakes behind both the SRWT and TRWT models at the downstream location of X/D = 2.0 were much higher than those of the incoming airflow. The elevated turbulence intensity levels are believed to be closely related to the generation and shedding of various unsteady vortex structures in the turbine wakes as visualized clearly in the "phase-locked" PIV measurements described above. It can also be seen that corresponding to the more complicated wake vortex structures in the TRWT wake, the turbulence intensity level in the TRWT wake was found to be much higher than that in the SRWT wake at the same downstream location of $X/D = 2.0$, especially in the region near the roots of the main rotor blades. The higher turbulence intensity levels in the TRWT wake would indicate more intensive turbulent mixing in the wake flow to promote a faster vertical transport process of kinetic energy from above to re-charge the low-momentum turbine wake flow, as suggested by Wu and Porte-Agel (2012), Calaf et al. (2010) and Cal et al. (2010). This would result in a faster recovery of the velocity deficits in the wake flow behind the TRWT model.

Due to the faster recovery of the velocity deficits in the far wake behind the TRWT model, the flow velocity in the TRWT wake at the downstream location of X/D = 4.0 was found to become greater than that in the SRWT wake, as shown in Fig. 11b. It suggests that the TRWT wake flow would become more energetic, in comparison with that of the SRWT case, at the same downstream location of X/D = 4.0. A higher wind power generation can be expected for a wind turbine sited in the wake behind a TRWT, in comparison with the case having the same turbine sited in the SRWT wake at the same downstream locations. It implies that the TRWT design can also be used to mitigate wake losses in wind farm settings. The measurement results given in Fig. 12b reveal that, while the turbulence intensity levels in the TRWT wake were still found to be much higher than those behind the SRWT model at the same downstream location of X/D = 4.0, the differences in the turbulence intensity profiles between the two compared cases were found to become smaller than those at the upstream location of X/D = 2.0.

As shown clearly in Fig. 11c, due to the more intensive turbulent mixing in the TRWT wake, the flow velocity, thereby, kinetic energy of the wake flow behind the TRWT model at the downstream location of X/D = 6.0 were found to become greater than those of the SRWT case. The measured turbulence intensity profiles given in Fig. 12c reveal that at the downstream location of X/D = 6.0, while the turbulence intensity levels in the TRWT wake were still found to be higher than those of in the SRWT wake, the differences between the two compared cases became much smaller, in comparison with those at the upstream locations. This suggests a shrinking differences in the wake velocity deficit recovery between the two compared cases at the further downstream locations of X/D > 6.0.

With the downstream distance increase further to X/D = 8.0, velocity deficits were still found to exist in the wake flows behind both the TRWT and SRWT models, as shown clearly in Fig. 11d. It indicates that in comparison with that of the incoming airflow, the flow velocity profiles in the turbine wakes have not been fully recovered yet even at the further downstream location of X/D = 8.0. However, the differences in the vertical profiles of streamwise velocity of the wake flows behind the TRWT and SRWT models were found to become very small at this downstream location. The measurement data given in Fig. 12d reveal that while the absolute values of the turbulence intensity levels in the turbine wake flows were found to decrease greatly and become almost comparable to those of the incoming airflow, the turbulence intensity levels in the wake flows behind the two compared turbine models were found to become almost the same at the downstream location of X/D = 8.0. Such measurement results suggest that the flow characteristics in the wakes behind the TRWT and SRWT model would become very similar at the further downstream region of X/D > 8.0. It also implies that the benefits of the TRWT design to augment turbulent mixing for a faster recovery of the velocity deficits in the turbine wake would fade away gradually in the further downstream region of X/D > 8.0.

Based on the transverse profiles as those shown in Figs. 11 and 12, the upper boundaries of the turbine wakes behind the turbine models can be identified easily, which are indicated as the dash lines in Fig. 11. Since the wake expansion rate behind the TRWT model is mainly determined by the larger primary rotor, the upper boundaries of the wakes behind the SRWT and TRWT models were found to be almost identical. Figure 13 shows the measured upper boundary location of the turbine wakes as a function of the downstream distance. As expected, the turbine wakes were found to expand monotonically with the increasing downstream distance. More specifically, as indicated in the plot, the relationship between the measured upper boundary location of the turbine wakes and the downstream distance away from the turbine rotor disk was found to be fitted well by a power function with the power-law exponent being about 2.0.

3.5 Comparison of the power outputs of the same downstream turbine sited in the wakes of the TRWT and SRWT models at different downstream locations

In the present study, a set of experiments were also conducted to directly measure and compare the power outputs of the same wind turbine model sited in the wake flows

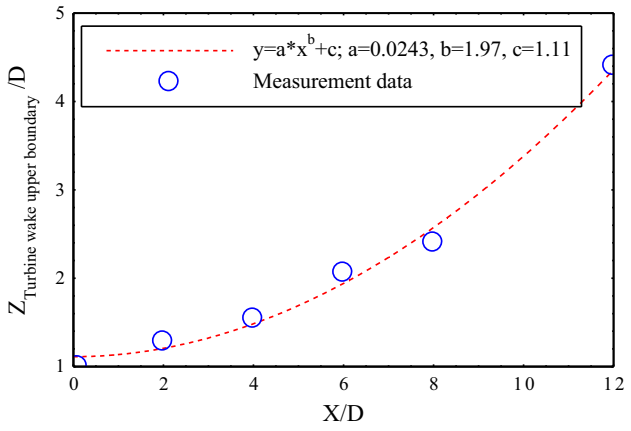

Fig. 13 The measured wake upper boundary location as a function of the downstream distance

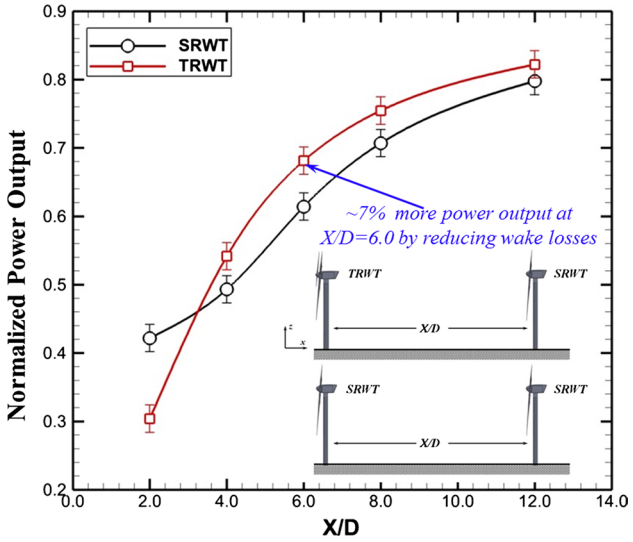

Fig. 14 Normalized power outputs of the downstream turbine model sited in the wakes behind the SRWT and TRWT models

behind the TRWT and SRWT models (i.e., aligned with the incoming airflow direction) at different downstream locations. The experimental study is aimed to simulate the worst scenario in wind farm settings to experience the greatest wake losses as reported in Bartherlmie et al. (2007, 2009). As described above, since the Reynolds numbers of the model turbines used in the present study are much smaller than those of utility-scale turbines operating in modern wind farms, the power coefficients of the small turbine models used in the present study (i.e., $C_P \approx$ 8–12 %) were found to be much lower than those of the utility-scale wind turbines (i.e., $C_P \approx$ 40–45 %). Instead of using absolute values of the power coefficients, normalized power outputs of the model turbines (i.e., normalized by the power output of the same turbine model operating in isolation without wake effects from upstream turbines) were used in the present study to reveal the characteristics of the power losses of the same downstream wind turbines due to the wake interference in typical wind farm settings, as suggest in Barthelmie et al. (2007).

Figure 14 gives the normalized power outputs of the same turbine model sited in the wakes behind the TRWT and SRWT models as a function of the downstream distance away from the upstream turbines. Corresponding to the significant velocity deficits in the wake flows behind the TRWT and SRWT models, the downstream turbine was found to experience significant wake losses due to the ingestion of the low-momentum wake flows of the upstream TRWT and SRWT models. The wake losses were found to be as high as 60–70 % when the downstream turbine model was sited at about 2.0 rotor diameters away from the upstream SRWT or TRWT model. As revealed from the vertical profiles of streamwise velocity given in Fig. 11, the velocity deficits in the turbine wakes would recover gradually as the downstream distance increases, the power losses of the downstream turbine due to the wake interference were found to become less and less as the downstream turbine moved further away from the upstream turbines. Based on the interpolation of the measurement results given in Fig. 14, the power loss of the downstream turbine due to the wake interference was found to be about 35, 27 and 23 %, respectively, as the distance between the upstream and downstream SRWT turbines being about 7.0D, 9.4D and 10.5D. The values of the wake losses were found to agree well with the field measurement data reported in Barthelmie et al. (2007), who measured the wake losses of conventional single-rotor wind turbines (i.e., SRWTs) sited in Horns Rev offshore wind farm.

The feasibility of using TRWT design to reduce the wake losses in typical wind farm settings was demonstrated clearly from the comparison of the measured power outputs of the same turbine sited in the wakes behind the SRWT and TRWT models, as given in Fig. 14. Due to the existence of the additional auxiliary rotor, the TRWT design would harness extra wind energy from the same incoming flow (i.e., by reducing the roots losses incurred in the region near the roots of the main rotor blades), in comparison with the conventional SRWT design. As a result, the velocity deficits in the near wake behind the TRWT model were found to be much more significant than those in the SRWT wake. With the turbine sited at the same downstream location of X/D = 2.0, corresponding to the much lower flow velocity in the near wake behind the TRWT model, the downstream turbine was found to have less power output when sited in the TRWT wake, in comparison with that in the SRWT wake, as expected. However, since the TRWT design with an extra auxiliary rotor can generate more

complicated wake vortex structures to augment the turbulent mixing in the TRWT wake, the velocity deficits in the far wake behind the TRWT model were found to recover much faster than that of the SRWT case. As a result, the magnitude of the flow velocity in the TRWT wake at the downstream location of X/D = 4.0 was found to become greater than that in the SRWT wake, as shown clearly in Fig. 11b. Corresponding to the higher wake flow velocity, thereby, more kinetic energy, in the TRWT wake at the downstream location of X/D = 4.0, the same downstream turbine model was found to be able to produce about 5 % more power when sited in the TRWT wake than that in the SRWT wake. It indicates that the TRWT design with an extra auxiliary rotor appended in front of the main rotor would not only be able to harness extra wind energy from the same incoming airflow (i.e., by reducing the root losses in the region near the roots of the main rotor blades), but also be capable of mitigating wake losses for downstream turbines in typical wind farm settings, in comparison with those of the conventional SRWT design.

The measurement results given in Fig. 14 also reveals that the benefits of the TRWT design in reducing the wake losses for the downstream turbines would be maximized when the spacing between the upstream and downstream turbines being about 6.0 rotor diameters, where the same downstream turbine model was found to be able to generate about 7 % more power when sited in the TRWT wake than that in the SRWT wake. With the downstream turbine model moving further away from the upstream turbine model, the advantage of the TRWT design over the conventional SRWT design in reducing the wake losses was found to shrink gradually, and the difference in the power outputs of the same downstream turbine between the two compared cases were found to become only about 2.5 % when the spacing between the upstream and downstream turbines being about 12.0 rotor diameters. The smaller and smaller benefits of the TRWT design in mitigating the wake losses in the far wake region of X/D > 8.0 was found to be correlated well with the continually shrinking differences in the flow velocity and turbulence intensity profiles behind the TRWT and SRWT models as shown in Figs. 11 and 12. It should be noted that the spacing between the upstream and downstream wind turbines is about 7–10 rotor diameters in a typical offshore wind farm, as described in Barthelmie et al. (2007). Based on the measurement data given in Fig. 14, with the spacing between the upstream and downstream wind turbines being 7–10 rotor diameters, the TRWT design with an extra auxiliary rotor appended in front of the main rotor would be able to improve the wind farm efficiency by mitigating the wake losses of the downstream turbines by about 4–6 %, in comparison with the conventional SRWT design.

4 Conclusion

An experimental study was conducted to characterize the aeromechanic performance and wake characteristics of a novel twin-rotor wind turbine (TRWT) concept for improved power production performance and wind farm efficiency. Unlike conventional single-rotor wind turbine (SRWT) design, the TRWT design employs an extra set of smaller, co-axial auxiliary rotor blades appended in front of the main rotor blades with two objectives: (1) reduce root losses incurred in the root region of the main rotor blades and (2) mitigate wake losses of downstream turbines in wind farm settings through enhanced turbulent mixing of turbine wake.

The experimental study was performed in a large-scale atmospheric boundary layer wind tunnel with scaled TRWT and SRWT models placed in the same incoming boundary layer airflow. In addition to measuring the dynamic wind loads acting on the model turbines, a digital particle image velocimetry (PIV) system was used to make detailed flow field measurements to quantify the wake flow characteristics and reveal the evolution of the unsteady wake vortices in the near wakes behind the TRWT and SRWT models. A Cobra Probe Anemometry system was also used to conduct velocity measurements in the far wake flows (i.e., in the downstream locations of X/D = 2.0–8.0) to supplement the PIV measurements. Furthermore, the power outputs of a model turbine sited in the wake behind the TRWT model at different downstream locations were also measured and compared quantitatively with those of the same model turbine sited in the wake behind the SRWT model.

The measurement results reveal clearly that while the TRWT design was found to be capable of harvesting more wind energy from the same incoming boundary layer flow by reducing the root losses of the main rotor blades, the dynamic wind loads acting on the TRWT model were found to be much greater (i.e., ~16 % increase in time-averaged wind loads, up to 140 % increase in the fluctuating amplitudes of the instantaneous wind loads) than those acting on the SRWT model. The much larger fluctuating amplitudes of the dynamic wind loads would indicate more significant fatigue loads acting on the TRWT model.

It was also found that due to the existence of the additional auxiliary rotor appended in front of the main rotor, the flow characteristics in the near wake behind the TRWT model were found to become significantly different (i.e., much larger velocity deficits in the near wake, more complex wake vortex structures, earlier breakdown of the concentrated wake vortices, and higher TKE and turbulent Reynolds stress levels), in comparison with those behind the SRWT model. Thanks to the more complex wake vortices generated behind the TRWT model, the turbulent

mixing process in the wake flow behind the TRWT model was found to be enhanced substantially, which greatly augment the vertical transport of kinetic energy by entraining more high-speed airflow from above to re-charge the low-momentum wake flow, causing a much faster recovery of the velocity deficits in the far wake behind the TRWT model. Therefore, the TRWT wake flow was found to become more energetic in the far wake region (i.e., X/D > 3.0) than that of the SRWT wake. As a result, the power outputs of a downstream turbine sited in the far wake behind the TRWT model were found be substantially greater than that of the same turbine sited in the wake behind a conventional SRWT model (i.e., up to 7 % more power output at the downstream location of 6.0 rotor diameters away from the upstream turbine). It indicates that the TRWT design with an extra auxiliary rotor would not only be able to harvest more energy from the same incoming wind by reducing the root losses of the main turbine rotor, but also be capable of improving wind farm efficiency by mitigating the wake losses for the downstream turbines through enhanced turbulent mixing of the turbine wake flows.

It should be noted that while the TRWT design were demonstrated to be capable of both improving turbine power production performance and mitigating wake losses in typical wind farm settings, the present experimental study was conducted in a wind tunnel with scaled wind turbine models. The corresponding Reynolds number of the scaled turbine models is about two orders lower than those of the utility-scale wind turbines, due to the inherent limitations of the wind tunnel testing with scaled model turbines. While the findings derived from the present study are believed to be very helpful to elucidate underlying physics related to aeromechanic characteristics of wind turbines, more comprehensive studies are still needed to explore/optimize design paradigms of TRWT design for higher power yield and better durability of the wind turbines operating in atmospheric boundary winds.

Acknowledgments The authors want to thank Mr. Bill Rickard of Iowa State University for helpful discussions in conducting for the present study. The funding support from the Iowa Energy Center with Grant No. 14-008-OG and National Science Foundation (NSF) with Grant Numbers of CBET-1133751 and CBET-1438099 is gratefully acknowledged.

References

Alfredsson PH, Dahlberg J-A, Vermeulen PEJ (1982) A comparison between predicted and measured data from wind turbine wakes. Wind Eng 6:149–155

Barthelmie RJ, Jensen LE (2010) Evaluation of wind farm efficiency and wind turbine wakes at the Nysted offshore wind farm. Wind Energ 13:573–586. doi:10.1002/we.408

Barthelmie RJ, Folkerts L, Ormel FT et al (2003) Offshore wind turbine wakes measured by sodar. J Atmos Ocean Technol 20:466–477. doi:10.1175/1520-0426(2003)20<466:OWTWMB>2.0.CO;2

Barthelmie RJ, Rathmann O, Frandsen ST et al (2007) Modelling and measurements of wakes in large wind farms. J Phys Conf Ser 75:012049. doi:10.1088/1742-6596/75/1/012049

Barthelmie RJ, Hansen K, Frandsen ST et al (2009) Modelling and measuring flow and wind turbine wakes in large wind farms offshore. Wind Energ 12:431–444. doi:10.1002/we.348

Barthelmie RJ, Pryor SC, Frandsen ST, Hansen KS, Schepers JG, Rados K, Schlez W, Neubert A, Jensen LE, Neckelmann S (2010) Quantifying the impact of wind turbine wakes on power output at offshore wind farms. J Atmos Ocean Technol 27:1302–1317

Burton T, Sharpe D, Jenkins N, Bossanyi E (2001) Wind energy handbook, 2nd edn. Wiley, New York

Cal RB, Lebrón J, Castillo L et al (2010) Experimental study of the horizontally averaged flow structure in a model wind-turbine array boundary layer. J Renew Sustain Energ 2:013106. doi:10.1063/1.3289735

Calaf M, Meneveau C, Meyers J (2010) Large eddy simulation study of fully developed wind-turbine array boundary layers. Phys Fluids 22:015110. doi:10.1063/1.3291077

Chamorro L, Porté-Agel F (2008) A wind tunnel investigation of wind turbine wakes: boundary-layer turbulence and surface roughness effects. Am Geophys Union Fall Meet, Abstr

Chamorro L, Porté-Agel F (2009) A wind-tunnel investigation of wind-turbine wakes: boundary-layer turbulence effects. Boundary-layer Meteorol 132:129–149

Chamorro LP, Porté-Agel F (2011) Turbulent flow inside and above a wind farm: a wind-tunnel study. Energies 4:1916–1936. doi:10.3390/en4111916

Chamorro LP, Arndt REA, Sotiropoulos F (2011) Turbulent flow properties around a staggered wind farm. Boundary-Layer Meteorol 141:349–367. doi:10.1007/s10546-011-9649-6

Chamorro LP, Arndt RE, Sotiropoulos F (2012) Reynolds number dependence of turbulence statistics in the wake of wind turbines. Wind Energ 15:733–742. doi:10.1002/we.501

Corten G, Lindenburg K, Schaak P (2007) Assembly of energy flow collectors, such as windpark, and method of operation. US Patent 7,299,627

Grant I, Parkin P (2000) A DPIV study of the trailing vortex elements from the blades of a horizontal axis wind turbine in yaw. Exp Fluids 28:368–376

Hansen KS, Barthelmie RJ, Jensen LE, Sommer A (2012) The impact of turbulence intensity and atmospheric stability on power deficits due to wind turbine wakes at Horns Rev wind farm. Wind Energ 15:183–196. doi:10.1002/we.512

Howard KB, Singh A, Sotiropoulos F, Guala M (2015) On the statistics of wind turbine wake meandering: an experimental investigation. Phys Fluids 27:075103. doi:10.1063/1.4923334

Hu H, Yang Z, Sarkar P (2011) Dynamic wind loads and wake characteristics of a wind turbine model in an atmospheric boundary layer wind. Exp Fluids 52:1277–1294. doi:10.1007/s00348-011-1253-5

Jain P (2010) Wind energy engineering, 1st edn. McGraw-Hill Professional, New York

Kaimal J, Finnigan J (1994) Atmospheric boundary layer flows: their structure and measurement. Oxford University Press, Oxford

Lebron J, Castillo L, Cal R (2010) Interaction between a wind turbine array and a turbulent boundary layer. In: AIAA2010-824, 448th AIAA aerospace science meeting including. New Horizons Forum Aerosp. Expo

Lignarolo LEM, Ragni D, Ferreira CJS, van Bussel GJW (2014) Kinetic energy entrainment in wind turbine and actuator disc wakes: an experimental analysis. J Phys Conf Ser 524:012163. doi:10.1088/1742-6596/524/1/012163

Locke J, Valencia U, Ishikawa K (2004) Design studies for twist-coupling wind turbine blades. Sandia National Laboratories, Technical Report No. SAND 2004–0522

Lu H, Porté-Agel F (2011) Large-eddy simulation of a very large wind farm in a stable atmospheric boundary layer. Phys Fluids 23:065101

Massouh F, Dobrev I (2007) Exploration of the vortex wake behind of wind turbine rotor. J Phys Conf Ser 75:012036. doi:10.1088/1742-6596/75/1/012036

Medici D (2005) Experimental studies of wind turbine wakes: power optimisation and meandering; KTH mechanics. Ph.D. thesis (KTH Mechanics, Royal Institute of Technology, Sweden. PhD Thesis, Royal Institute of Technology

Meyers J, Meneveau C (2012) Optimal turbine spacing in fully developed wind farm boundary layers. Wind Energ 15:305–317. doi:10.1002/we.469

Ozbay A, Tian W, Yang Z, Hu H (2012) An experimental investigation on the wake interference of multiple wind turbines in atmospheric boundary layer winds. In: AIAA Pap. 2012-2784, 30th AIAA applied aerodynamic conference 25–28 June 2012, New Orleans, Louisiana

Røkenes K (2009) Investigation of terrain effects with respect to wind farm siting. PhD thesis, Department of Energy and Process Engineering, Norwegian University of Science and Technology

Rosenberg A, Selvaraj S, Sharma A (2014) A novel dual-rotor turbine for increased wind energy capture. J Phys Conf Ser 524:012078. doi:10.1088/1742-6596/524/1/012078

Ross JN, Ainslie JF (1981) Wake measurements in clusters of model wind turbines using laser Doppler anemometry. In Proceedings Third BWEA Wind Energy Conference Cranfield, UK, pp 172–184

Selvaraj S, Chaves A, Takle E, Sharma A (2013) Numerical prediction of surface flow convergence phenomenon in wind farms. Conf Wind Energ Sci Technol

Sescu A, Meneveau C, Sescu A, Meneveau C (2015) Large-eddy simulation and single-column modeling of thermally stratified wind turbine arrays for fully developed. Station Atmos Cond. doi:10.1175/JTECH-D-14-00068.1

Sherry M, Nemes A, Lo Jacono D et al (2013) The interaction of helical tip and root vortices in a wind turbine wake. Phys Fluids 25:117102. doi:10.1063/1.4824734

Storm B, Dudhia J, Basu S et al (2009) Evaluation of the weather research and forecasting model on forecasting low-level jets: implications for wind energy. Wind Energ 12:81–90. doi:10.1002/we.288

Tian W, Ozbay A, Hu H (2014) Effects of incoming surface wind conditions on the wake characteristics and dynamic wind loads acting on a wind turbine model. Phys Fluids 26:125108. doi:10.1063/1.4904375

Tong W (2010) Wind Power Generation and Wind Turbine Design. WIT Press, England

Vermeer L, Sørensen J, Crespo A (2003) Wind turbine wake aerodynamics. Prog Aerosp Sci 39:476–510

Wan T, Wu S (2004) Aerodynamic analysis under influence of heavy rain. J Aeronaut Astronaut Aviat 173–180

Whale J, Anderson C An experimental investigation of wind turbine wakes using particle image velocimetry. In: Proceedings of 1993 European Community Wind Energy Conference, Lubeck-Travemunde, Germany, pp 457–460

Whale J, Anderson C, Bareiss R, Wagner S (2000) An experimental and numerical study of the vortex structure in the wake of a wind turbine. J Wind Eng Ind Aerodyn 84:1–21. doi:10.1016/S0167-6105(98)00201-3

Wu Y-T, Porté-Agel F (2012) atmospheric turbulence effects on wind-turbine wakes: an LES study. Energies 5:5340–5362. doi:10.3390/en5125340

Wu Y-T, Porté-Agel F (2015) Modeling turbine wakes and power losses within a wind farm using LES: an application to the Horns Rev offshore wind farm. Renew Energ 75:945–955. doi:10.1016/j.renene.2014.06.019

Xie S, Archer C (2015) Self-similarity and turbulence characteristics of wind turbine wakes via large-eddy simulation. Wind Energ 18:1815–1838. doi:10.1002/we.1792

Yang Z, Sarkar P, Hu H (2011) Visualization of the tip vortices in a wind turbine wake. J Vis 15:39–44. doi:10.1007/s12650-011-0112-z

Yuan W, Tian W, Ozbay A, Hu H (2014) An experimental study on the effects of relative rotation direction on the wake interferences among tandem wind turbines. Sci China Phys Mech Astron 57:935–949. doi:10.1007/s11433-014-5429-x

Zhou Y, Kareem A (2002) Definition of wind profiles in ASCE 7. J Struct Eng 128:1082–1086. doi:10.1061/(ASCE)0733-9445(2002)128:8(1082)